

# A Unified Framework for 3D Scene Understanding

Wei Xu\*, Chunsheng Shi\*, Sifan Tu, Xin Zhou, Dingkang Liang, Xiang Bai†  
 Huazhong University of Science and Technology  
 {wxu2023, csshi, tuska, xzhou03, dkliang, xbai}@hust.edu.cn

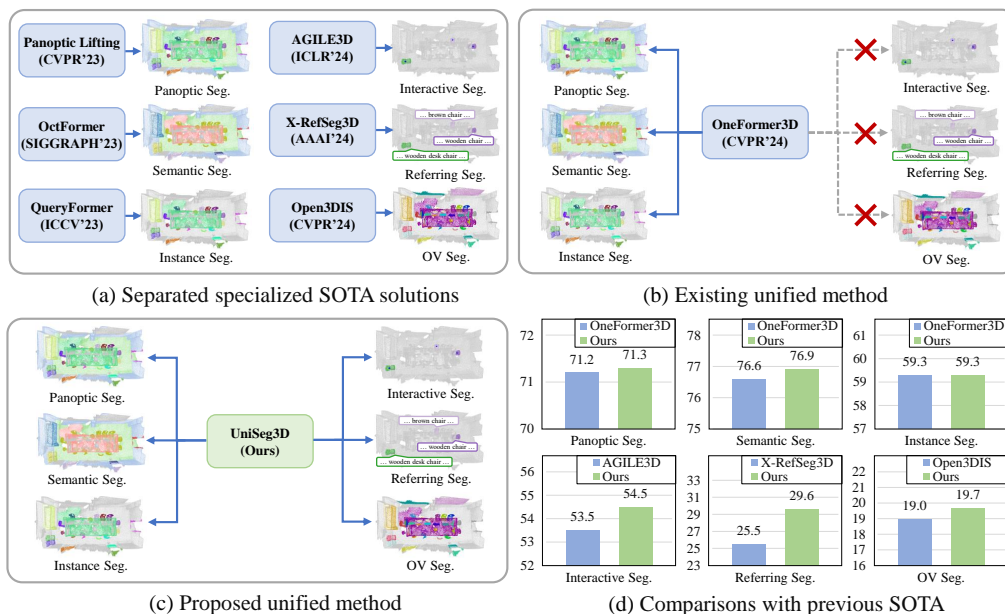


Figure 1: Comparisons between the proposed method and current SOTA approaches specialized for specific tasks. (a) Representative specialized approaches on six tasks. (b) Oneformer3D, a recent unified framework, achieves SOTA performance on three generic segmentation tasks in once inference. (c) The proposed unified framework achieves six tasks in once inference. (d) Our method outperforms current SOTA approaches across six tasks involving two modalities using a single model.

## Abstract

We propose UniSeg3D, a unified 3D segmentation framework that achieves panoptic, semantic, instance, interactive, referring, and open-vocabulary semantic segmentation tasks within a single model. Most previous 3D segmentation approaches are specialized for a specific task, thereby limiting their understanding of 3D scenes to a task-specific perspective. In contrast, the proposed method unifies six tasks into unified representations processed by the same Transformer. It facilitates inter-task knowledge sharing and, therefore, promotes comprehensive 3D scene understanding. To take advantage of multi-task unification, we enhance the performance by leveraging task connections. Specifically, we design a knowledge distillation method and a contrastive learning method to transfer task-specific knowledge across different tasks. Benefiting from extensive inter-task knowledge sharing, our UniSeg3D becomes more powerful. Experiments on three benchmarks, including the ScanNet20, ScanRefer, and ScanNet200, demonstrate that the UniSeg3D consistently outperforms current SOTA methods, even those specialized for individual tasks. We hope UniSeg3D can serve as a solid unified baseline and inspire future work. The code will be available at <https://dk-liang.github.io/UniSeg3D/>.

\*Equal contribution. †Corresponding author.

# 1 Introduction

3D scene understanding has been a foundational aspect of various real-world applications [3, 62, 15], including robotics, autonomous navigation, and mixed reality. Among the 3D scene understanding tasks, the 3D point cloud segmentation is a crucial component. Generic 3D point cloud segmentation contains instance, semantic, and panoptic segmentation (IS/SS/PS) tasks [33, 37, 52, 60, 18], which segment classes annotated in the training set. As a complement, 3D open-vocabulary semantic segmentation (OVS) task [36, 48] segments open-vocabulary classes of interest. Another group of researches study to utilize the user priors. In particular, 3D interactive segmentation task [20, 61] segments instances specified by users. 3D referring segmentation task [13, 40] segments instances described by textual expressions. The above mentioned tasks are core tasks in 3D scene understanding, drawing significant interest from researchers and achieving great success.

Previous studies [47, 8, 65, 16] in the 3D scene understanding area focus on separated solutions specialized for specific tasks, as shown in Fig. 1(a). These approaches ignore the intrinsic connections across different tasks, such as the geometric consistency and semantic consistency of the objects. They also fail to share knowledge that is biased toward other tasks, limiting their understanding of 3D scenes to a task-specific perspective. This poses significant challenges for achieving comprehensive and in-depth 3D scene understanding. A recent exploration [19] named OneFormer3D designs an architecture to unify the 3D generic segmentation tasks, as shown in Fig. 1(b). This architecture inputs instance and semantic queries to achieve the 3D instance and semantic segmentation simultaneously. And the 3D panoptic segmentation is subsequently achieved by post-processing. It is simple yet effective. However, this architecture fails to support the 3D interactive segmentation, 3D referring segmentation, and OVS tasks, which provide complementary scene information including user priors and open-set classes, should be consistently crucial in the 3D scene understanding as the generic segmentation tasks. This leads to a natural consideration that *if these 3D scene understanding tasks can be unified in a single framework?*

A direct solution is to integrate the separated methods into a single architecture. However, it faces challenges in balancing the customized optimizations specialized for the specific tasks involved in these methods. Thus, we aim to design a simple and elegant framework without task-specific customized modules. This inspires us to design the UniSeg3D, a unified framework processing six 3D segmentation tasks in parallel. Specifically, we use queries to unify the representation of the input information. For the 3D generic segmentation tasks and the OVS task, which only input the point cloud without human knowledge, thus can be processed sharing the same workflow without worrying about prior knowledge leakage. We use one unified set of queries to represent the four-task features for simplification. The interactive segmentation inputs the visual point priors to condition the segmentation. We represent the point prompt information by simply sampling the point cloud queries, thereby avoiding repeated point feature extraction. The referring segmentation inputs textual expressions, which persist modality gap with the point clouds and are hard to be unified into the previous workflows. To minimize the time consumption, we design a parallel text prompt encoder to extract the text queries. All these queries are decoded using the same mask decoder and share the same output head, thereby avoiding the design of task-specific customized structures.

We further enhance the performance by taking advantage of the multi-task design. In particular, we empirically find that the interactive segmentation outperforms the rest of the tasks in mask predictions attributing to the reliable vision priors. Hence, we design a knowledge distillation method to distill the knowledge from the interactive segmentation to the other tasks. Then, we build contrastive learning between the interactive segmentation and referring segmentation to connect these two tasks. The proposed knowledge distillation and contrastive learning promote knowledge sharing across six tasks, facilitating a comprehensive and in-depth 3D scene understanding. There are three significant strengths of the UniSeg3D: (1) it unifies six 3D scene understanding tasks in a single framework, as shown in Fig. 1(c); (2) it is flexible for that can be easily extended to more tasks by simply inputting the additional task-specific queries; (3) the designed knowledge distillation and contrastive learning are only used in the training phase, optimizing the performance with no extra inference cost.

We compare the proposed method with task-specific specialized SOTA approaches [45, 50, 31, 61, 40, 35] across six tasks to evaluate its performance. As shown in Fig. 1(d), the UniSeg3D demonstrates superior performance on all the tasks. It is worth noting that our performance on different tasks is achieved by a single model, which is more efficient than running separate task-specific approaches individually. Furthermore, the structure of UniSeg3D is simple and elegant, containing no task-

customized modules, while consistently outperforming specialized SOTA solutions, demonstrating a desirable potential to be a solid unified baseline.

In general, our contributions can be summarized as follows: **First**, we propose a unified framework named UniSeg3D, which is a flexible and efficient solution for 3D scene understanding. It achieves six 3D segmentation tasks in once inference by a single model. To the best of our knowledge, this is the first work unifying six 3D segmentation tasks. **Second**, specialized approaches limit their 3D scene understanding to task-specific perspectives. We facilitate the inter-task knowledge sharing to promote comprehensive 3D scene understanding. Specifically, we take advantage of the multi-task unification, designing the knowledge distillation and contrastive learning methods to build inter-task associations explicitly.

## 2 Related Work

**3D segmentation.** The generic segmentation consists of panoptic, semantic, and instance segmentation. The panoptic segmentation [33, 51] is the union of the instance segmentation [9, 28, 2, 55, 49] and semantic segmentation [39, 37, 5, 63]. It contains the instance masks from the instance segmentation and the stuff masks from the semantic segmentation. These 3D segmentation tasks rely on annotations, segmenting classes labeled in the training set. The open-vocabulary semantic segmentation [35, 48] extends the 3D segmentation to the novel class. Another group of researches explores 3D segmentation conditioned by the human knowledge. Specifically, the interactive segmentation [20, 61] segments instances specified by the point clicks. The referring segmentation [13, 40] segments objects described by textual expressions. Most previous researches [56, 4, 21, 27] focus on specific 3D segmentation tasks, limiting their efficiency in multi-task scenarios, such as the domotics, that require multiple task-specific 3D segmentation approaches to be applied simultaneously. In this work, we propose a framework to achieve the above mentioned six tasks in a single prediction.

**Unified vision models.** Unified researches support multiple tasks in a single model, facilitating the efficiency and having attracted a lot of attention in the 2D area [38, 32, 25, 14]. However, rare works study the unified 3D segmentation architecture. It probably attributes to the higher dimension of the 3D data, which leads to a big solution space, making it challenging for sufficient unification across multiple 3D tasks. Recent works [11, 30] explore outdoor unified 3D segmentation architectures. So far, only one method, OneFormer3D [19], focuses on indoor unified 3D segmentation. It extends the motivation proposed in OneFormer [14] to the 3D area and proposes an architecture to achieve three 3D generic segmentation tasks in a single model. We note that the supported tasks in OneFormer3D can be achieved in once inference through post-processing predictions of a panoptic segmentation model. In contrast, we propose a simple framework to unify six tasks, including not only generic segmentation but also interactive segmentation, referring segmentation, and OVS into a single model. We further propose to build explicit associations between the unified tasks to facilitate knowledge sharing across them, contributing to an effective multi-task unification.

## 3 Methodology

The framework of UniSeg3D is depicted in Fig. 2. It primarily consists of three modules: a point cloud backbone, prompt encoders, and a mask decoder. We illustrate their structures in the following.

### 3.1 Point Cloud Backbone and Prompt Encoders

**Point cloud backbone.** We formulate the set of  $N$  input points as  $\mathbf{P} \in \mathbb{R}^{N \times 6}$ , where each point is parameterized with three-dimensional coordinates  $x, y, z$  and three-channel colors  $r, g, b$ . Then, the input points are fed into a sparse 3D U-Net as the point cloud backbone to obtain point-wise features  $\mathbf{F} \in \mathbb{R}^{N \times d_{in}}$ , where  $d_{in}$  is the feature dimension. In the 3D scene understanding applications, individual processing of dense points would be time-consuming. Thus, we downsample the 3D scenario into  $M$  superpoints, pooling point features within these superpoints into superpoint features  $\mathbf{F}_s = \{\mathbf{f}_i\}_{i=1}^M$  where  $\mathbf{f}_i \in \mathbb{R}^{d_{in}}$ , which exhibit awareness of the edge textures [23] while reducing cost consumption.

**Vision prompt encoder.** Clicked point is a kind of clear and convenient visual interaction condition, which has been widely employed in previous works [17, 20, 61]. We formulate the clicked points as

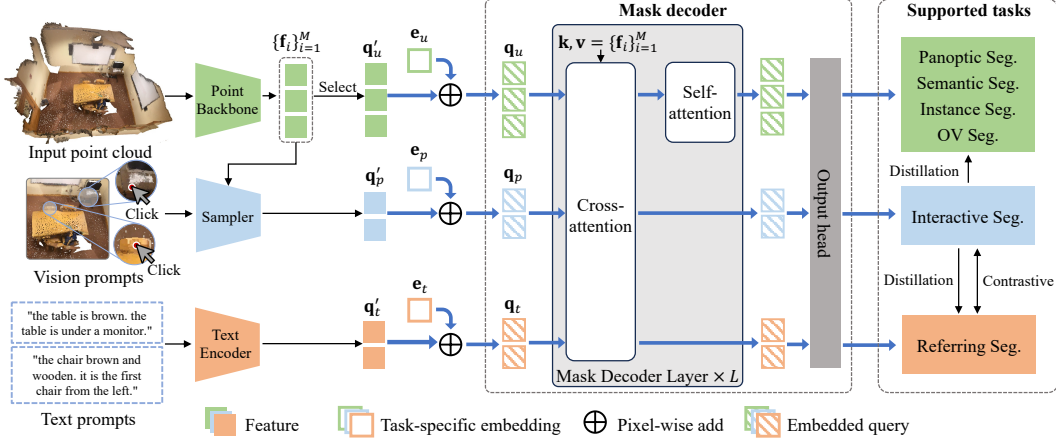


Figure 2: The framework of UniSeg3D. The UniSeg3D processes six tasks in parallel. This is a simple framework with no modules specialized for specific tasks. We take advantage of multi-task unification and enhance the performance through building associations between the supported tasks, *i.e.*, the knowledge distillation transfers knowledge from the interactive segmentation to the rest of the tasks. The contrastive learning connects the interactive segmentation and the referring segmentation.

the vision prompts, as illustrated in Fig. 2. As the whole 3D scenario is divided into superpoints, the point prompt must be located at some of the superpoints. We sample the corresponding superpoint feature as the point prompt embedding  $\mathbf{f}_p \in \mathbb{R}^{d_{in}}$  to represent the point prompt information, thus avoiding redundant feature extraction and maintaining feature consistency with the point clouds.

**Text prompt encoder.** The UniSeg3D is able to segment instances described by textual expressions. To process a text prompt, the initial step involves tokenizing the text sentence to obtain its string tokens  $\mathbf{T} \in \mathbb{R}^{l \times c}$ , where  $l$  is the sentence length and  $c$  represents the token dimension. These tokens are then fed into a frozen CLIP [41] text encoder to produce a  $C$ -dimension text embedding  $\mathbf{f}_t \in \mathbb{R}^C$ . This embedding is subsequently projected by two linear layers into the  $d_{in}$  dimension, obtaining  $\mathbf{f}_t \in \mathbb{R}^{d_{in}}$ , aligning it with the dimensions of the point features for further processing.

### 3.2 Mask Decoder

We employ a single mask decoder to output predictions of six 3D scene understanding tasks. Specifically, the generic segmentation and the OVS share the same input data, *i.e.*, the point cloud without user knowledge. We serve unified queries  $\mathbf{q}'_u \in \mathbb{R}^{m \times d_{in}}$  for both the generic segmentation and OVS tasks, where  $m$  is the number of the queries. The unified queries are randomly selected from the superpoint features. For conciseness, we set  $m < M$  in the training phase and  $m = M$  for the inference.

The prompt information is encoded into prompt embedding as discussed in Sec. 3.1. We employ the prompt embeddings as the prompt queries, which can be written as:  $\mathbf{q}'_p = \{\mathbf{f}_{p,i}\}_{i=1}^{K_p}$ ,  $\mathbf{q}'_t = \{\mathbf{f}_{t,i}\}_{i=1}^{K_t}$ , where  $\mathbf{q}'_p \in \mathbb{R}^{K_p \times d_{in}}$ ,  $\mathbf{q}'_t \in \mathbb{R}^{K_t \times d_{in}}$ .  $K_p$  and  $K_t$  are the number of the point and text prompts, respectively.  $\mathbf{q}'_u, \mathbf{q}'_p, \mathbf{q}'_t$  are three types of queries containing information from various aspects. Feeding them forward indiscriminately would confuse the mask decoder for digging task-specific information. Thus, we add task-specific embeddings  $\mathbf{e}_u, \mathbf{e}_p$ , and  $\mathbf{e}_t$  before further processing:

$$\mathbf{q}_u = \mathbf{q}'_u + \mathbf{e}_u, \quad \mathbf{q}_p = \mathbf{q}'_p + \mathbf{e}_p, \quad \mathbf{q}_t = \mathbf{q}'_t + \mathbf{e}_t, \quad (1)$$

where  $\mathbf{e}_u \in \mathbb{R}^{d_{in}}$ ,  $\mathbf{e}_p \in \mathbb{R}^{d_{in}}$ ,  $\mathbf{e}_t \in \mathbb{R}^{d_{in}}$ , and are broadcasted into  $\mathbb{R}^{m \times d_{in}}$ ,  $\mathbb{R}^{K_p \times d_{in}}$ , and  $\mathbb{R}^{K_t \times d_{in}}$ , respectively. The mask decoder comprises  $L$  mask decoder layers, which contain self-attention layers integrating information among queries. Prompt priors are unavailable for generic segmentation during inference. Therefore, in the training phase, we should prevent the human knowledge from leaking to the generic segmentation. In practice, the prompt queries are exclusively fed into the cross-attention layers. Output queries of the last mask decoder layer are sent into an output head, which consists of MLP layers to project dimensions  $d_{in}$  of the output queries into  $d_{out}$ . In general, the mask decoder



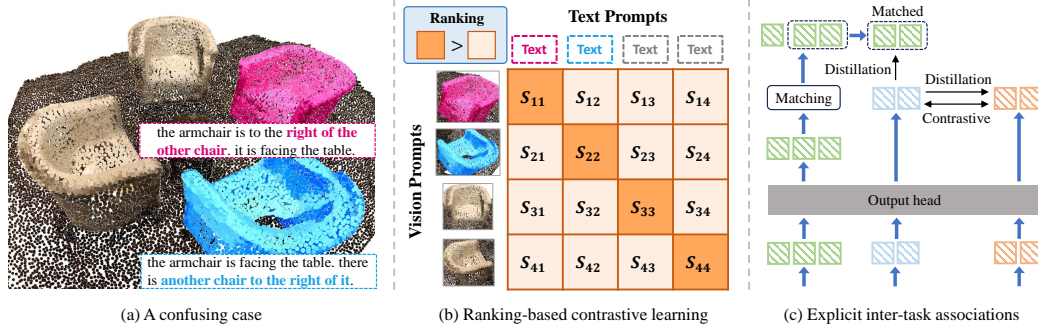


Figure 3: Illustration of the inter-task association. (a) A confusing case where requiring to distinguish the textual position information involved in the expressions. (b) A contrastive learning matrix for the vision-text pairs. The ranking rule is designed to suppress the incorrect pairs. (c) Knowledge distillations between multi-task predictions.

can be formally defined as:

$$\mathbf{F}_{out} = \text{MaskDecoder}(\mathbf{q} = \text{Concat}(\mathbf{q}_u, \mathbf{q}_p, \mathbf{q}_t); \mathbf{k} = \mathbf{F}_s; \mathbf{v} = \mathbf{F}_s), \quad (2)$$

where  $\mathbf{F}_{out} = \{\mathbf{f}_{out,i}\}_{i=1}^{m+K_p+K_t}$  represents the output features and  $\mathbf{f}_{out,i} \in \mathbb{R}^{d_{out}}$ .

Subsequently, we can process the output features to obtain the class and mask predictions. For the class predictions, a common practice is replacing class names with class IDs [19]. However, for our method to achieve the referring segmentation, the class names are essential information that should not be ignored. Hence, we propose to regress the class name embeddings  $\mathbf{e}_{cls} \in \mathbb{R}^{K_v \times d_{out}}$  instead, where  $K_v$  is the number of categories in vocabularies. In particular, we formulate the mask predictions  $\text{mask}_{pred}$  and class predictions  $\text{cls}_{pred}$  as follows:

$$\text{mask}_{pred} = \mathbf{F}_{out} \times \text{MLP}(\mathbf{F}_s)^\top, \quad \text{cls}_{pred} = \text{Softmax}(\mathbf{f}_{out} \times \mathbf{e}_{cls}^\top), \quad (3)$$

where  $\text{mask}_{pred} = \{\text{mask}_i\}_{i=1}^{m+K_p+K_t}$  and  $\text{cls}_{pred} = \{\text{cls}_i\}_{i=1}^{m+K_p+K_t}$ .  $\text{mask}_i \in \mathbb{R}^m$  represents the  $i$ -th predicted segmentation mask and  $\text{cls}_i \in \mathbb{R}^{K_v}$  represents the  $i$ -th category probability. The MLP projects  $\mathbb{R}^{d_{in}}$  into  $\mathbb{R}^{d_{out}}$ . To the end, during inference, we inverse map the superpoints to the original point clouds to obtain the final mask predictions and class predictions.

### 3.3 Explicit Inter-task Association

Associations among 3D scene understanding tasks have been overlooked in previous studies. It leads to a result that the task-specific approaches can not perceive across-task knowledge, limiting the understanding of the 3D scenes to a task-specific perspective. This limitation barriers comprehensive 3D scene understanding. Thus, we build explicit inter-task associations to break this limitation.

Specifically, on the one hand, as shown in Fig. 3(a), the referring segmentation is challenging when multiple individuals of identical shapes are arranged adjacently. It requires the method to distinguish the location variations involved in the text prompts, such as ‘right of the other chair’ vs. ‘another chair to the right of it’. However, the modality gap between the point and text modalities set significant barriers. We propose ranking-based contrastive learning between the vision and text features to reduce the modality gap and optimize the referring segmentation.

On the other hand, as shown in Tab. 1, the mIoU metric measures the quality of mask predictions directly, we observe that the interactive segmentation task equips with superior mask prediction performance. We attribute it to the reliable position priors from the vision prompts. Consequently, we transfer knowledge from the interactive segmentation to the rest of the tasks to guide the training phase.

Table 1: Mask prediction performance of interactive segmentation.

task	mIoU
Interactive Seg.	76.0

#### 3.3.1 Ranking-based Contrastive Learning

We set the point and text prompts specifying the same individual instances into pairs and align their pair-wise features by employing contrastive learning.

Assuming  $B$  text-point pairs within a training mini-batch, the corresponding output features are  $\{\mathbf{f}_{out,i}^p\}_{i=1}^B$  and  $\{\mathbf{f}_{out,i}^t\}_{i=1}^B$ , where  $\mathbf{f}_{out,i}^p$  and  $\mathbf{f}_{out,i}^t$  are selected from output features  $\{\mathbf{f}_{out,i}\}_{i=m+1}^{m+K_p}$  and  $\{\mathbf{f}_{out,i}\}_{i=m+K_p+1}^{m+K_p+K_t}$ , respectively. We normalize the pair-wise point-text output features  $\{\mathbf{f}_{out,i}^p\}_{i=1}^B$  and  $\{\mathbf{f}_{out,i}^t\}_{i=1}^B$  and obtain the metric embeddings  $\{\mathbf{e}_i^p\}_{i=1}^B$  and  $\{\mathbf{e}_i^t\}_{i=1}^B$ , respectively. We formulate the contrastive learning loss as  $\mathcal{L}_{con} = \mathcal{L}_p + \mathcal{L}_t$ , with:

$$\mathcal{L}_p = -\frac{1}{B} \sum_{i=1}^B \log \frac{\exp(\mathbf{e}_i^p \mathbf{e}_i^t / \tau)}{\sum_{j=1}^B \exp(\mathbf{e}_i^p \mathbf{e}_j^t / \tau)}, \quad \mathcal{L}_t = -\frac{1}{B} \sum_{i=1}^B \log \frac{\exp(\mathbf{e}_i^t \mathbf{e}_i^p / \tau)}{\sum_{j=1}^B \exp(\mathbf{e}_i^t \mathbf{e}_j^p / \tau)}, \quad (4)$$

where  $\tau$  is a learnable temperature. The pair-wise similarity can be depicted in Fig. 3(b), where we denote  $\mathbf{e}_i^p \mathbf{e}_j^t$  as  $\mathbf{s}_{i,j}$  for simplification. To distinguish the target instances from adjacent ones with identical shapes, we introduce a ranking rule inspired by the CrowdCLIP [26] that the diagonal elements are greater than the off-diagonal elements, which can be described as:

$$\mathcal{L}_{rank} = \frac{1}{B} \sum_{i=1}^B \sum_{j=1}^B \max(0, \mathbf{s}_{i,j} - \mathbf{s}_{i,i}). \quad (5)$$

### 3.3.2 Knowledge Distillation

As shown in Fig. 3(c), we transfer knowledge from the interactive task to the generic and referring tasks to guide their training phases.

**Interactive segmentation to the generic segmentation task.** Define the predictions by the unified queries as  $\text{Pred}_u = \{\text{mask}_i, \text{cls}_i\}_{i=1}^m$ . We employ the Hungarian algorithm, utilizing the Dice and cross-entropy metrics as the matching cost criteria to assign  $\text{Pred}_u$  with the interactive segmentation labels  $\text{GT}_p = \{\text{mask}_i^{gt}, \text{cls}_i^{gt}\}_{i=1}^{K_p}$ , and obtain the positive samples as  $\text{Pos}_u = \{\text{mask}_i^{pos}, \text{cls}_i^{pos}\}_{i=1}^{K_p}$ . The predicted masks by the interactive segmentation can be formulated as  $\text{mask}_p = \{\text{mask}_i\}_{i=m+1}^{m+K_p} \in \mathbb{R}^{K_p \times m}$ . We select the pixels with top  $k\%$  scores as learning region  $\mathbf{R} \subseteq \text{mask}_p$ , and depict the knowledge transfer process from the interactive segmentation to the generic segmentation task as:

$$\mathcal{L}_{p \rightarrow g} = \mathcal{L}_{BCE}(\text{mask}_{pos}(\mathbf{R}), \text{mask}_p(\mathbf{R})), \quad (6)$$

where  $\text{mask}_{pos}(\mathbf{R})$  and  $\text{mask}_p(\mathbf{R})$  represent the estimated mask values gathered in the region  $\mathbf{R}$  from the positive samples and the interactive segmentation predictions, respectively.

**Interactive segmentation to the referring segmentation task.** Define the pair-wise class probabilities predicted by the point and text queries as  $\text{cls}_p$  and  $\text{cls}_t$ , respectively. We formulate a knowledge transfer process from the interactive segmentation to the referring segmentation task as

$$\mathcal{L}_{p \rightarrow r} = \mathcal{L}_{BCE}(\text{Sigmoid}(\text{cls}_t), \text{Sigmoid}(\text{cls}_p)). \quad (7)$$

## 3.4 Training Objectives

**Open-set pseudo mask labels.** For the open-vocabulary tasks, the methods are trained on the close set. To enhance the segmentation performance on the open-set, we use SAM3D [58] to generate pseudo segmentation masks with undetermined categories. Specifically, as discussed in Sec. 3.2, the positive samples are used to regress the close-set masks. For the negative samples, we match them with the pseudo segmentation masks and select the matched ones to regress the pseudo labels. Note that the SAM3D is an unsupervised method and uses no ground-truth annotations, which means there are no worries about label leakage. And this process is only employed during the training phase, which does not increase the inference cost.

**Loss function.** The training losses contain two components: (1) the basic losses, formulated as  $\mathcal{L}_{base} = \mathcal{L}_{mask} + \mathcal{L}_{cls}$ .  $\mathcal{L}_{mask}$  stands for pixel-wise mask loss, which comprises of the BCE loss and the Dice loss.  $\mathcal{L}_{cls}$  indicates the classification loss, where we use the cross-entropy loss. (2) the losses used to build inter-task associations, summarized as  $\mathcal{L}_{inter} = \mathcal{L}_{p \rightarrow g} + \mathcal{L}_{p \rightarrow r} + \mathcal{L}_{con} + \mathcal{L}_{rank}$ . The final loss function is  $\mathcal{L} = \mathcal{L}_{base} + \lambda \mathcal{L}_{inter}$ , where  $\lambda$  is a balance weight, setting as 0.1.

Table 2: Comparisons on **ScanNet20** [6], **ScanRefer** [1], and **ScanNet200** [42]. The best results are in **bold** while the second best results are underscored. ‘\*’ means using the two-stage fine-tuning trick. ‘-/-’ denotes training on the filtered or complete ScanRefer dataset, respectively.

Datasets		ScanNet20				ScanRefer	ScanNet200
3D scene understanding tasks		PS	SS	IS	Interactive	Referring	OVS
Method	Reference	PQ	mIoU	mAP	AP	mIoU	AP
SceneGraphFusion [51]	CVPR’21	31.5	-	-	-	-	-
TUPPer-Map [59]	IROS’21	50.2	-	-	-	-	-
Panoptic Lifting [45]	CVPR’23	58.9	-	-	-	-	-
PanopticNDT [44]	IROS’23	59.2	-	-	-	-	-
PointNeXt-XL [39]	NeurIPS’22	-	71.5	-	-	-	-
PointMetaBase-XXL [29]	CVPR’23	-	72.8	-	-	-	-
MM-3DScene [57]	CVPR’23	-	72.8	-	-	-	-
PointTransformerV2 [53]	NeurIPS’22	-	75.4	-	-	-	-
ADS [10]	ICCV’23	-	75.6	-	-	-	-
OctFormer [50]	SIGGRAPH’23	-	75.7	-	-	-	-
SoftGroup [49]	CVPR’22	-	-	45.8	-	-	-
PBNet [64]	ICCV’23	-	-	54.3	-	-	-
ISBNet [34]	CVPR’23	-	-	54.5	-	-	-
SPFormer [46]	AAAI’23	-	-	56.3	-	-	-
Mask3D [43]	ICRA’23	-	-	55.2	-	-	-
MAFT [22]	ICCV’23	-	-	58.4	-	-	-
QueryFormer [31]	ICCV’23	-	-	56.5	-	-	-
OneFormer3D [19]	CVPR’24	<u>71.2</u>	<u>76.6</u>	<b>59.3</b>	-	-	-
InterObject3D [20]	ICRA’23	-	-	-	20.9	-	-
AGILE3D [61]	ICLR’24	-	-	-	53.5	-	-
TGNN [13]	AAAI’21	-	-	-	-	24.9/27.8	-
X-RefSeg3D [40]	AAAI’24	-	-	-	-	25.5/29.9	-
OpenScene [36] + Mask3D [43]	CVPR’23	-	-	-	-	-	8.5
OpenMask3D [48]	NeurIPS’23	-	-	-	-	-	12.6
SOLE [24]	CVPR’24	-	-	-	-	-	18.7
Open3DIS [35]	CVPR’24	-	-	-	-	-	19.0
UniSeg3D (ours)	-	<b>71.3</b>	76.3	<u>59.1</u>	<u>54.1</u>	29.5/-	<u>19.6</u>
UniSeg3D* (ours)	-	<b>71.3</b>	<b>76.9</b>	<b>59.3</b>	<b>54.5</b>	<b>29.6/-</b>	<b>19.7</b>

## 4 Experiments

**Datasets.** We evaluate the UniSeg3D on three benchmarks: ScanNet20 [6], ScanNet200 [42], and ScanRefer [1]. ScanNet20 provides RGB-D images and 3D point clouds of 1,613 scenes, including 18 instance categories and 2 semantic categories. ScanNet200 uses the same source data as the ScanNet20, while it is more challenging for up to 198 instance categories and 2 semantic categories. ScanRefer contains 51,583 natural language expressions referring to 11,046 objects selected from 800 scenes.

**Experimental setups.** We train our method on the ScanNet20 training split, and the referring texts are collected from the ScanRefer. The  $d_{in}$  and  $d_{out}$  are set as 32 and 256, respectively.  $m$  ranges [50, 100] percents of  $M$  with an upper limit of 3,500. We set  $k$  as 10 and  $L$  as 6. For the data augmentations, the point clouds are randomly flipped horizontally, rotated around the z-axis, elastic distorted, and scaled; the referring texts are augmented using public GPT tools following [54, 7]. We adopt the AdamW optimizer with the polynomial schedule, setting an initial learning rate as 0.0001 and the weight decay as 0.05. All models are trained for 512 epochs on a single NVIDIA RTX 4090 GPU and evaluated per 16 epochs on the validation set to find the best-performed model. To stimulate the performance, we propose a two-stage fine-tuning trick, which fine-tunes the best-performed model using the learning rate and weight decay 0.001 times the initial values for 40 epochs. The proposed framework achieves end-to-end generic, interactive, and referring segmentation tasks. We divide the OVS task into mask prediction and class prediction. Specifically, we employ the proposed UniSeg3D to predict masks and then follow the Open3DIS [35] to generate class predictions.

Table 3: Ablation on components. ‘Distillation’, ‘Rank-Contrastive’, and ‘Trick’ denote the knowledge distillation, ranking-based contrastive learning, and two-stage fine-tuning trick, respectively.

Datasets			ScanNet20			ScanRefer	ScanNet200	
Components			PS	SS	IS	Interactive	Referring	OVS
Distillation	Rank-Contrastive	Trick	PQ	mIoU	mAP	AP	mIoU	AP
-	-	-	70.4	76.2	58.0	<u>54.5</u>	29.1	<u>19.7</u>
✓	-	-	<u>71.2</u>	76.2	<b>59.3</b>	<b>56.6</b>	29.2	19.6
-	✓	-	70.8	<u>76.4</u>	58.4	54.1	<b>29.6</b>	<b>20.2</b>
✓	✓	-	<b>71.3</b>	76.3	<u>59.1</u>	54.1	<u>29.5</u>	19.6
✓	✓	✓	<b>71.3</b>	<b>76.9</b>	<b>59.3</b>	<u>54.5</u>	<b>29.6</b>	<u>19.7</u>

Table 4: Ablation on different designs of the proposed components. ‘ $p \rightarrow g$ ’ and ‘ $p \rightarrow r$ ’ denote the knowledge distillation from the interactive segmentation to the generic segmentation and the referring segmentation, respectively. ‘Contrastive’ and ‘Rank’ denote the contrastive learning and the ranking rule, respectively.

(a) Ablation on designs for knowledge distillation.								(b) Ablation on designs for ranking-based contrastive learning.							
$p \rightarrow g$	$p \rightarrow r$	PS	SS	IS	Interactive	Referring	OVS	Contrastive	Rank	PS	SS	IS	Interactive	Referring	OVS
-	-	70.8	<b>76.4</b>	58.4	<b>54.1</b>	<u>29.6</u>	<b>20.2</b>	-	-	<u>71.2</u>	<u>76.2</u>	<b>59.3</b>	<b>56.6</b>	29.2	19.6
✓	-	<b>71.4</b>	<u>76.3</u>	<u>59.0</u>	<u>54.0</u>	<u>29.6</u>	19.8	✓	-	70.9	<b>76.3</b>	59.0	53.8	<u>29.4</u>	<u>19.7</u>
-	✓	70.7	76.2	58.4	<b>54.1</b>	<b>29.7</b>	<u>20.1</u>	-	✓	70.8	<u>76.2</u>	58.6	53.4	<u>29.4</u>	<b>19.8</b>
✓	✓	<u>71.3</u>	<u>76.3</u>	<b>59.1</b>	<b>54.1</b>	29.5	19.6	✓	✓	<b>71.3</b>	<b>76.3</b>	<u>59.1</u>	54.1	<b>29.5</b>	19.6

Table 5: Ablation on hyper-parameter  $\lambda$ .

$\lambda$	PS	SS	IS	Interactive	Referring	OVS
0.05	70.7	76.2	<u>58.9</u>	<b>54.4</b>	29.5	<b>19.6</b>
0.1	<b>71.3</b>	<u>76.3</u>	<b>59.1</b>	54.1	29.5	<b>19.6</b>
0.2	<u>70.8</u>	<b>76.6</b>	58.6	<u>52.3</u>	<b>29.8</b>	<u>19.5</u>
0.3	70.6	75.7	58.4	51.6	<u>29.6</u>	19.3

Table 6: Ablation on task unification.

OVS	Referring	Interactive	PS	SS	IS
AP	mIoU	AP	PQ	mIoU	mAP
<b>X</b>	<b>X</b>	<b>X</b>	<b>71.0</b>	76.2	<b>59.0</b>
<b>X</b>	<b>X</b>	56.8	<b>71.0</b>	<b>76.4</b>	<u>58.7</u>
<b>X</b>	29.1	56.0	70.3	<u>76.3</u>	58.4
19.7	29.1	54.5	<u>70.4</u>	76.2	58.0

As for the metrics, we use the PQ, mIoU, and mAP to evaluate performance on the generic tasks following [33, 37, 60]. Then, we use the AP and mIoU for the interactive and referring segmentation tasks, respectively, following [61, 40]. For the OVS task, we train our model on the ScanNet20 and evaluate it using the AP metric on the ScanNet200 without specific fine-tuning, following [48].

#### 4.1 Comparison to the SOTA Methods

The proposed method achieves six 3D scene understanding tasks in a single model. We demonstrate the effectiveness of our method by comparing it with SOTA approaches specialized for specific tasks. As shown in Tab. 2, the proposed method outperforms the specialized SOTA methods Panoptic-NDT [44], OctFormer [50], MAFT [22], AGILE3D [61], X-RefSeg3D [40], and Open3DIS [35] on the PS, SS, IS, interactive segmentation, referring segmentation, and OVS tasks by 12.1 PQ, 1.2 mIoU, 0.9 mAP, 1.0 AP, 4.1 mIoU, 0.7 AP, respectively. Even when compared with the competitive 3D unified method, *i.e.*, OneFormer3D [19], the proposed UniSeg3D achieves 0.1 PQ improvement on the PS task, and 0.3 mIoU improvement on the SS task. More importantly, the OneFormer3D focuses on three generic segmentation tasks. It fails to understand user prompts and is unable to achieve OVS, which limits its application prospects. In contrast, the UniSeg3D unifies six tasks and demonstrates desirable performance across all of them. This illustrates that the UniSeg3D is a powerful architecture.

The proposed method achieves six tasks in once training, which is elegant while facing an issue for fair comparison that part of the labels (10, 115 objects, 27.6 percent of the complete ScanRefer training set) in the referring segmentation benchmark belongs to the novel classes of the open-vocabulary segmentation task. Obviously, these labels should not be used for training to avoid label leakage. Thus, we filter out this part of labels and only employ the filtered ScanRefer training set to train our model. As we can see in Tab. 2, the proposed method use 72.4 percent of the training data to

achieve closing performance with X-RefSeg3D [40] (29.6 vs. 29.9), the current specialized SOTA on the 3D referring segmentation task. Moreover, while we reproduce the X-RefSeg3D using official code on the same set of filtered training data, the performance drops to 4.1 mIoU lower than ours. It demonstrates the effectiveness of our method on the referring segmentation task.

## 4.2 Analysis and Ablation

We conduct ablation studies and analyze the key insights of our designs. All models are evaluated on unified tasks to better show the effectiveness of the proposed components on wide scopes.

**Design of inter-task associations.** In our approach, we use knowledge distillation and contrastive learning to connect supported tasks. As shown in Tab. 3, when applying the distillation, *i.e.* row 2, the performance of IS and interactive segmentation increase to 59.3 mAP and 56.6 AP, respectively. We believe the improvement on the IS is because of the reliable knowledge distilled from the interactive segmentation, and the improvement on interactive segmentation is attributed to the intrinsic connections between the two tasks. Then, we ablate the ranking-based contrastive learning, *i.e.* row 3. We observe improvements on four tasks, including the generic segmentation and the referring segmentation, while a bit of performance drop on the interactive segmentation. This phenomenon suggests that the contrastive learning is effective in most tasks while there is a huge struggle to align the point and text modalities, which weakens the interactive segmentation performance. Applying the knowledge distillation and the ranking-based contrastive learning simultaneously obtains comparable performance on six tasks, indicating the complementarity of the two components. We further employ the two-stage fine-tuning trick, bringing consistent improvements across various tasks.

Detailed ablation on the components is shown in Tab. 4. It is observed that knowledge distillation to various tasks brings respective improvements. As for the contrastive learning, comparing row 2 and row 4 in Tab. 4(b), the ranking rule suppresses the confusing point-text pairs, boosting the contrastive learning to be more effective.  $\lambda$  controls the strength of the explicit inter-task associations. We empirically find that setting  $\lambda$  to 0.1 obtains the best performance, as shown in Tab. 5.

**Influence of task unification.** The proposed framework is flexible and can be conveniently extended to additional tasks. As shown in Tab. 6, we ablate the number of unified tasks and observe a continuous performance decline on the PS, IS, and interactive segmentation. It demonstrates a significant challenge in balancing different tasks.

**Influence of vision prompts.** We empirically find that the vision prompts affect the interactive segmentation performance. For a fair comparison, we use the same vision prompts generated by the AGILE3D [61] to evaluate our interactive segmentation performance.

Furthermore, to analysis the influence of vision prompts, we ablate the 3D spatial distances between the vision prompts and the instance centers. Specifically, assuming an instance containing  $n$  points, we denote the mean coordinate of these points as the instance center and order the  $n$  points based on their distances to the instance center. Then, we evaluate the interactive segmentation performance while using the  $\lfloor D \times n \rfloor$ -th nearest point as the vision prompt, as shown in Tab. 7. When the vision prompt is located at the instance center, the interactive segmentation achieves the upper bound performance of 56.6 AP. There is a significant performance gap (up to 20.2 AP) between the edge point and center point. It illustrates considerable room for improvement. We observe an unusual decline in AP while converting  $D$  from 0.9 to 1.0. We think this is because of the ambiguity to distinguish the edge points from adjacent instances. As we all know, this is the first work ablating the influence. We will explore it deeply in the future work.

Table 7: Ablation on vision prompts.

Ratio $\tau_d$	mIoU	AP	AP <sub>50</sub>	AP <sub>25</sub>
From [61]	78.8	54.5	79.4	93.2
Upper Bound	<b>79.6</b>	<b>56.6</b>	<b>82.1</b>	<b>94.9</b>
0.1	<u>79.1</u>	<u>55.9</u>	<u>81.1</u>	<u>94.4</u>
0.2	78.7	55.1	80.0	93.4
0.3	78.0	53.8	78.5	92.4
0.4	77.5	53.0	77.4	91.7
0.5	76.6	52.1	76.2	90.6
0.6	75.9	51.2	74.6	90.0
0.7	74.9	50.1	72.9	88.1
0.8	73.4	48.2	71.1	86.5
0.9	71.0	45.3	66.6	82.1
1.0	62.7	36.4	54.8	70.2
Random	76.0	51.3	75.2	89.6

## 5 Conclusion and Discussion

We design a unified framework named UniSeg3D, which offers a flexible and efficient solution for 3D scene understanding, supporting six tasks within a single model. Previous task-specific approaches



fail to extract across-task information, limiting their understanding of 3D scenes to a task-specific perspective. In contrast, we take advantage of the multi-task design and enhance the performance through building inter-task associations. Specifically, we propose the knowledge distillation and ranking-based contrastive to facilitate across-task knowledge sharing. Experiments demonstrate that the proposed framework is powerful and achieves SOTA performance on all six unified tasks.

**Limitation.** The proposed method aims to achieve unified 3D scene understanding. However, this work focuses on indoor tasks, and lacks discussions in outdoor scenes. The modality gap between the 3D point cloud and the linguistic texts is still significant, leading to performance discrepancy between the 3D interactive segmentation and the 3D referring segmentation. For the interactive segmentation task, we find out that UniSeg3D performs worse when the vision prompt is located away from the instance centers. It limits the reliability of the UniSeg3D and should be explored in the future work.

## References

- [1] Dave Zhenyu Chen, Angel X Chang, and Matthias Nießner. Scanrefer: 3d object localization in rgb-d scans using natural language. In *Proc. of European Conference on Computer Vision*, pages 202–221, 2020.
- [2] Shaoyu Chen, Jiemin Fang, Qian Zhang, Wenyu Liu, and Xinggang Wang. Hierarchical aggregation for 3d instance segmentation. In *Proc. of IEEE Intl. Conf. on Computer Vision*, pages 15467–15476, 2021.
- [3] Shizhe Chen, Ricardo Garcia, Ivan Laptev, and Cordelia Schmid. Sugar: Pre-training 3d visual representations for robotics. In *Proc. of IEEE Intl. Conf. on Computer Vision and Pattern Recognition*, pages 18049–18060, 2024.
- [4] Silin Cheng, Xiwu Chen, Xinwei He, Zhe Liu, and Xiang Bai. Pra-net: Point relation-aware network for 3d point cloud analysis. *IEEE Transactions on Image Processing*, 30:4436–4448, 2021.
- [5] Christopher Choy, JunYoung Gwak, and Silvio Savarese. 4d spatio-temporal convnets: Minkowski convolutional neural networks. In *Proc. of IEEE Intl. Conf. on Computer Vision and Pattern Recognition*, pages 3075–3084, 2019.
- [6] Angela Dai, Angel X. Chang, Manolis Savva, Maciej Halber, Thomas Funkhouser, and Matthias Nießner. ScanNet: Richly-annotated 3D reconstructions of indoor scenes. In *Proc. of IEEE Intl. Conf. on Computer Vision and Pattern Recognition*, pages 5828–5839, 2017.
- [7] Haixing Dai, Zhengliang Liu, Wenxiong Liao, Xiaoke Huang, Yihan Cao, Zihao Wu, Lin Zhao, Shaochen Xu, Wei Liu, Ninghao Liu, et al. Auggpt: Leveraging chatgpt for text data augmentation. *arXiv preprint arXiv:2302.13007*, 2023.
- [8] Lei Han, Tian Zheng, Lan Xu, and Lu Fang. Occuseg: Occupancy-aware 3d instance segmentation. In *Proc. of IEEE Intl. Conf. on Computer Vision and Pattern Recognition*, pages 2940–2949, 2020.
- [9] Tong He, Chunhua Shen, and Anton Van Den Hengel. Dyco3d: Robust instance segmentation of 3d point clouds through dynamic convolution. In *Proc. of IEEE Intl. Conf. on Computer Vision and Pattern Recognition*, pages 354–363, 2021.
- [10] Cheng-Yao Hong, Yu-Ying Chou, and Tyng-Luh Liu. Attention discriminant sampling for point clouds. In *Proc. of IEEE Intl. Conf. on Computer Vision*, pages 14429–14440, 2023.
- [11] Fangzhou Hong, Lingdong Kong, Hui Zhou, Xinge Zhu, Hongsheng Li, and Ziwei Liu. Unified 3d and 4d panoptic segmentation via dynamic shifting networks. *IEEE Transactions on Pattern Analysis and Machine Intelligence*, 2024.
- [12] Ji Hou, Angela Dai, and Matthias Nießner. 3d-sis: 3d semantic instance segmentation of rgb-d scans. In *Proc. of IEEE Intl. Conf. on Computer Vision and Pattern Recognition*, pages 4421–4430, 2019.
- [13] Pin-Hao Huang, Han-Hung Lee, Hwann-Tzong Chen, and Tyng-Luh Liu. Text-guided graph neural networks for referring 3d instance segmentation. In *Proc. of the AAAI Conf. on Artificial Intelligence*, pages 1610–1618, 2021.
- [14] Jitesh Jain, Jiachen Li, Mang Tik Chiu, Ali Hassani, Nikita Orlov, and Humphrey Shi. Oneformer: One transformer to rule universal image segmentation. In *Proc. of IEEE Intl. Conf. on Computer Vision and Pattern Recognition*, pages 2989–2998, 2023.
- [15] Maximilian Jaritz, Jiayuan Gu, and Hao Su. Multi-view pointnet for 3d scene understanding. In *Proceedings of the IEEE/CVF international conference on computer vision workshops*, pages 0–0, 2019.
- [16] Li Jiang, Hengshuang Zhao, Shaoshuai Shi, Shu Liu, Chi-Wing Fu, and Jiaya Jia. Pointgroup: Dual-set point grouping for 3d instance segmentation. In *Proc. of IEEE Intl. Conf. on Computer Vision and Pattern Recognition*, pages 4867–4876, 2020.

- [17] Alexander Kirillov, Eric Mintun, Nikhila Ravi, Hanzi Mao, Chloe Rolland, Laura Gustafson, Tete Xiao, Spencer Whitehead, Alexander C Berg, Wan-Yen Lo, et al. Segment anything. In *Proc. of IEEE Intl. Conf. on Computer Vision*, pages 4015–4026, 2023.
- [18] Maksim Kolodiaznyi, Danila Rukhovich, Anna Vorontsova, and Anton Konushin. Top-down beats bottom-up in 3d instance segmentation. *arXiv preprint arXiv:2302.02871*, 2023.
- [19] Maxim Kolodiaznyi, Anna Vorontsova, Anton Konushin, and Danila Rukhovich. Oneformer3d: One transformer for unified point cloud segmentation. In *Proc. of IEEE Intl. Conf. on Computer Vision and Pattern Recognition*, 2024.
- [20] Theodora Kontogianni, Ekin Celikkan, Siyu Tang, and Konrad Schindler. Interactive object segmentation in 3d point clouds. In *Proc. of the IEEE Int. Conf. on Robot. and Automat.*, pages 2891–2897, 2023.
- [21] Xin Lai, Jianhui Liu, Li Jiang, Liwei Wang, Hengshuang Zhao, Shu Liu, Xiaojuan Qi, and Jiaya Jia. Stratified transformer for 3d point cloud segmentation. In *Proc. of IEEE Intl. Conf. on Computer Vision and Pattern Recognition*, 2022.
- [22] Xin Lai, Yuhui Yuan, Ruihang Chu, Yukang Chen, Han Hu, and Jiaya Jia. Mask-attention-free transformer for 3d instance segmentation. In *Proc. of IEEE Intl. Conf. on Computer Vision*, pages 3693–3703, 2023.
- [23] Loic Landrieu and Martin Simonovsky. Large-scale point cloud semantic segmentation with superpoint graphs. In *Proc. of IEEE Intl. Conf. on Computer Vision and Pattern Recognition*, pages 4558–4567, 2018.
- [24] Seungjun Lee, Yuyang Zhao, and Gim Hee Lee. Segment any 3d object with language. In *Proc. of IEEE Intl. Conf. on Computer Vision and Pattern Recognition*, 2024.
- [25] Xiangtai Li, Haobo Yuan, Wei Li, Henghui Ding, Size Wu, Wenwei Zhang, Yining Li, Kai Chen, and Chen Change Loy. Omg-seg: Is one model good enough for all segmentation? In *Proc. of IEEE Intl. Conf. on Computer Vision and Pattern Recognition*, 2024.
- [26] Dingkan Liang, Jiahao Xie, Zhikang Zou, Xiaoqing Ye, Wei Xu, and Xiang Bai. Crowdclip: Unsupervised crowd counting via vision-language model. In *Proc. of IEEE Intl. Conf. on Computer Vision and Pattern Recognition*, pages 2893–2903, 2023.
- [27] Dingkan Liang, Xin Zhou, Xinyu Wang, Xingkui Zhu, Wei Xu, Zhikang Zou, Xiaoqing Ye, and Xiang Bai. Pointmamba: A simple state space model for point cloud analysis. *arXiv preprint arXiv:2402.10739*, 2024.
- [28] Zhihao Liang, Zhihao Li, Songcen Xu, Mingkui Tan, and Kui Jia. Instance segmentation in 3d scenes using semantic superpoint tree networks. In *Proc. of IEEE Intl. Conf. on Computer Vision*, pages 2783–2792, 2021.
- [29] Haojia Lin, Xiawu Zheng, Lijiang Li, Fei Chao, Shanshan Wang, Yan Wang, Yonghong Tian, and Rongrong Ji. Meta architecture for point cloud analysis. In *Proc. of IEEE Intl. Conf. on Computer Vision and Pattern Recognition*, pages 17682–17691, 2023.
- [30] Youquan Liu, Lingdong Kong, Xiaoyang Wu, Runnan Chen, Xin Li, Liang Pan, Ziwei Liu, and Yuexin Ma. Multi-space alignments towards universal lidar segmentation. In *Proc. of IEEE Intl. Conf. on Computer Vision and Pattern Recognition*, 2024.
- [31] Jiahao Lu, Jiacheng Deng, Chuxin Wang, Jianfeng He, and Tianzhu Zhang. Query refinement transformer for 3d instance segmentation. In *Proc. of IEEE Intl. Conf. on Computer Vision*, pages 18516–18526, 2023.
- [32] Li Minghan, Li Shuai, Zhang Xindong, and Zhang Lei. Univs: Unified and universal video segmentation with prompts as queries. In *Proc. of IEEE Intl. Conf. on Computer Vision and Pattern Recognition*, 2024.
- [33] Gaku Narita, Takashi Seno, Tomoya Ishikawa, and Yohsuke Kaji. Panopticfusion: Online volumetric semantic mapping at the level of stuff and things. In *IEEE Int. Workshop on Intelligent Robots and Systems*, pages 4205–4212, 2019.
- [34] Tuan Duc Ngo, Binh-Son Hua, and Khoi Nguyen. Isbnet: a 3d point cloud instance segmentation network with instance-aware sampling and box-aware dynamic convolution. In *Proc. of IEEE Intl. Conf. on Computer Vision and Pattern Recognition*, pages 13550–13559, 2023.
- [35] Phuc DA Nguyen, Tuan Duc Ngo, Chuang Gan, Evangelos Kalogerakis, Anh Tran, Cuong Pham, and Khoi Nguyen. Open3dis: Open-vocabulary 3d instance segmentation with 2d mask guidance. In *Proc. of IEEE Intl. Conf. on Computer Vision and Pattern Recognition*, 2024.
- [36] Songyou Peng, Kyle Genova, Chiyu Jiang, Andrea Tagliasacchi, Marc Pollefeys, Thomas Funkhouser, et al. Openscene: 3d scene understanding with open vocabularies. In *Proc. of IEEE Intl. Conf. on Computer Vision and Pattern Recognition*, pages 815–824, 2023.
- [37] Charles Ruizhongtai Qi, Li Yi, Hao Su, and Leonidas J Guibas. Pointnet++: Deep hierarchical feature learning on point sets in a metric space. In *Proc. of Advances in Neural Information Processing Systems*, 2017.

- [38] Lu Qi, Lehan Yang, Weidong Guo, Yu Xu, Bo Du, Varun Jampani, and Ming-Hsuan Yang. Unigs: Unified representation for image generation and segmentation. In *Proc. of IEEE Intl. Conf. on Computer Vision and Pattern Recognition*, 2024.
- [39] Guocheng Qian, Yuchen Li, Houwen Peng, Jinjie Mai, Hasan Hammoud, Mohamed Elhoseiny, and Bernard Ghanem. Pointnext: Revisiting pointnet++ with improved training and scaling strategies. In *Proc. of Advances in Neural Information Processing Systems*, pages 23192–23204, 2022.
- [40] Zhipeng Qian, Yiwei Ma, Jiayi Ji, and Xiaoshuai Sun. X-refseg3d: Enhancing referring 3d instance segmentation via structured cross-modal graph neural networks. In *Proc. of the AAAI Conf. on Artificial Intelligence*, pages 4551–4559, 2024.
- [41] Alec Radford, Jong Wook Kim, Chris Hallacy, Aditya Ramesh, Gabriel Goh, Sandhini Agarwal, Girish Sastry, Amanda Askell, Pamela Mishkin, Jack Clark, et al. Learning transferable visual models from natural language supervision. In *Proc. of Intl. Conf. on Machine Learning*, pages 8748–8763, 2021.
- [42] David Rozenberszki, Or Litany, and Angela Dai. Language-grounded indoor 3d semantic segmentation in the wild. In *Proc. of European Conference on Computer Vision*, pages 125–141, 2022.
- [43] Jonas Schult, Francis Engelmann, Alexander Hermans, Or Litany, Siyu Tang, and Bastian Leibe. Mask3d: Mask transformer for 3d semantic instance segmentation. In *Proc. of the IEEE Int. Conf. on Robot. and Automat.*, pages 8216–8223, 2023.
- [44] Daniel Seichter, Benedict Stephan, Söhnke Benedikt Fishedick, Steffen Müller, Leonard Rabes, and Horst-Michael Gross. Panopticndt: Efficient and robust panoptic mapping. In *IEEE Int. Workshop on Intelligent Robots and Systems*, pages 7233–7240, 2023.
- [45] Yawar Siddiqui, Lorenzo Porzi, Samuel Rota Buló, Norman Müller, Matthias Nießner, Angela Dai, and Peter Kotschieder. Panoptic lifting for 3d scene understanding with neural fields. In *Proc. of IEEE Intl. Conf. on Computer Vision and Pattern Recognition*, pages 9043–9052, 2023.
- [46] Jiahao Sun, Chunmei Qing, Junpeng Tan, and Xiangmin Xu. Superpoint transformer for 3d scene instance segmentation. In *Proc. of the AAAI Conf. on Artificial Intelligence*, volume 37, pages 2393–2401, 2023.
- [47] Weiwei Sun, Daniel Rebain, Renjie Liao, Vladimir Tankovich, Soroosh Yazdani, Kwang Moo Yi, and Andrea Tagliasacchi. Neuralbf: Neural bilateral filtering for top-down instance segmentation on point clouds. In *Proc. of IEEE Winter Conf. on Applications of Computer Vision*, pages 551–560, 2023.
- [48] Ayca Takmaz, Elisabetta Fedele, Robert Sumner, Marc Pollefeys, Federico Tombari, and Francis Engelmann. Openmask3d: Open-vocabulary 3d instance segmentation. In *Proc. of Advances in Neural Information Processing Systems*, 2023.
- [49] Thang Vu, Kookhoi Kim, Tung M Luu, Thanh Nguyen, and Chang D Yoo. Softgroup for 3d instance segmentation on point clouds. In *Proc. of IEEE Intl. Conf. on Computer Vision and Pattern Recognition*, pages 2708–2717, 2022.
- [50] Peng-Shuai Wang. Octformer: Octree-based transformers for 3d point clouds. *ACM Transactions ON Graphics*, 42(4):1–11, 2023.
- [51] Shun-Cheng Wu, Johanna Wald, Keisuke Tateno, Nassir Navab, and Federico Tombari. Scenegrphfusion: Incremental 3d scene graph prediction from rgb-d sequences. In *Proc. of IEEE Intl. Conf. on Computer Vision and Pattern Recognition*, pages 7515–7525, 2021.
- [52] Wenxuan Wu, Zhongang Qi, and Li Fuxin. Pointconv: Deep convolutional networks on 3d point clouds. In *Proc. of IEEE Intl. Conf. on Computer Vision and Pattern Recognition*, pages 9621–9630, 2019.
- [53] Xiaoyang Wu, Yixing Lao, Li Jiang, Xihui Liu, and Hengshuang Zhao. Point transformer v2: Grouped vector attention and partition-based pooling. In *Proc. of Advances in Neural Information Processing Systems*, pages 33330–33342, 2022.
- [54] Yanmin Wu, Qiankun Gao, Renrui Zhang, and Jian Zhang. Language-assisted 3d scene understanding. In *Proc. of the AAAI Conf. on Artificial Intelligence*, 2024.
- [55] Yizheng Wu, Min Shi, Shuaiyuan Du, Hao Lu, Zhiguo Cao, and Weicai Zhong. 3d instances as 1d kernels. In *Proc. of European Conference on Computer Vision*, pages 235–252, 2022.
- [56] Chenfeng Xu, Bichen Wu, Zining Wang, Wei Zhan, Peter Vajda, Kurt Keutzer, and Masayoshi Tomizuka. Squeeze3d: Spatially-adaptive convolution for efficient point-cloud segmentation. In *Proc. of European Conference on Computer Vision*, pages 1–19, 2020.
- [57] Mingye Xu, Mutian Xu, Tong He, Wanli Ouyang, Yali Wang, Xiaoguang Han, and Yu Qiao. Mm-3dscene: 3d scene understanding by customizing masked modeling with informative-preserved reconstruction and self-distilled consistency. In *Proc. of IEEE Intl. Conf. on Computer Vision and Pattern Recognition*, pages 4380–4390, 2023.
- [58] Yunhan Yang, Xiaoyang Wu, Tong He, Hengshuang Zhao, and Xihui Liu. Sam3d: Segment anything in 3d scenes. *arXiv preprint arXiv:2306.03908*, 2023.

- [59] Zhiliu Yang and Chen Liu. Tupper-map: Temporal and unified panoptic perception for 3d metric-semantic mapping. In *IEEE Int. Workshop on Intelligent Robots and Systems*, pages 1094–1101, 2021.
- [60] Li Yi, Wang Zhao, He Wang, Minhyuk Sung, and Leonidas J Guibas. Gspn: Generative shape proposal network for 3d instance segmentation in point cloud. In *Proc. of IEEE Intl. Conf. on Computer Vision and Pattern Recognition*, pages 3947–3956, 2019.
- [61] Yuanwen Yue, Sabarinath Mahadevan, Jonas Schult, Francis Engelmann, Bastian Leibe, Konrad Schindler, and Theodora Kontogianni. Agile3d: Attention guided interactive multi-object 3d segmentation. In *Proc. of Intl. Conf. on Learning Representations*, 2024.
- [62] Dingyuan Zhang, Dingkang Liang, Hongcheng Yang, Zhikang Zou, Xiaoqing Ye, Zhe Liu, and Xiang Bai. Sam3d: Zero-shot 3d object detection via segment anything model. *Science China Information Sciences*, 2023.
- [63] Hengshuang Zhao, Li Jiang, Jiaya Jia, Philip HS Torr, and Vladlen Koltun. Point transformer. In *Proc. of IEEE Intl. Conf. on Computer Vision*, pages 16259–16268, 2021.
- [64] Weiguang Zhao, Yuyao Yan, Chaolong Yang, Jianan Ye, Xi Yang, and Kaizhu Huang. Divide and conquer: 3d point cloud instance segmentation with point-wise binarization. In *Proc. of IEEE Intl. Conf. on Computer Vision*, pages 562–571, 2023.
- [65] Xin Zhou, Dingkang Liang, Wei Xu, Xingkui Zhu, Yihan Xu, Zhikang Zou, and Xiang Bai. Dynamic adapter meets prompt tuning: Parameter-efficient transfer learning for point cloud analysis. In *Proceedings of the IEEE/CVF Conference on Computer Vision and Pattern Recognition*, pages 14707–14717, 2024.

## Appendix

In this appendix, we provide additional content to complement the main manuscript:

- Appendix A: Comparisons employing more metrics on specific tasks.
- Appendix B: Analysis on the inference time of the proposed UniSeg3D.
- Appendix C: Qualitative visualizations in more 3D scenarios.

### A Comparisons with Approaches Specialized for Specific Tasks.

The experiments presented in the main manuscript primarily utilize the overall metrics each task. This section provides a comprehensive comparison of each task using more detailed metrics. The performance of 3D open-vocabulary semantic segmentation is assessed on the ScanNet200 by utilizing masks generated from UniSeg3D trained on ScanNet20. Following[35], 51 classes that are semantically close to the ScanNet20 categories are grouped as “Base”, while the remaining classes are grouped as “Novel”.

Table I: For comparison with existing instance segmentation methods, we test our approach on ScanNet, achieving performance that is competitive with state-of-the-art.

Method	Reference	Instance		
		mAP <sub>25</sub>	mAP <sub>50</sub>	mAP
3D-SIS[12]	CVPR'19	35.7	18.7	-
GSPN[60]	CVPR'19	53.4	37.8	19.3
PointGroup[16]	CVPR'20	71.3	56.7	34.8
OccuSeg[8]	CVPR'20	71.9	60.7	44.2
DyCo3D[9]	CVPR'21	72.9	57.6	35.4
SSTNet[28]	ICCV'21	74.0	64.3	49.4
HAIS[2]	ICCV'21	75.6	64.4	43.5
DKNet[55]	ICCV'22	76.9	66.7	50.8
SoftGroup[49]	CVPR'22	78.9	67.6	45.8
PBNet[64]	ICCV'23	78.9	70.5	54.3
ISBNet[34]	CVPR'23	82.5	73.1	54.5
SPFormer[46]	AAAI'23	82.9	73.9	56.3
Mask3D[43]	ICRA'23	83.5	73.7	55.2
MAFT[22]	ICCV'23	-	75.9	<u>58.4</u>
QueryFormer[31]	ICCV'23	83.3	74.2	56.5
OneFormer3D[19]	CVPR'24	<b>86.4</b>	<b>78.1</b>	<b>59.3</b>
UniSeg3D (ours)	-	<u>86.1</u>	<u>77.0</u>	<b>59.3</b>

Table II: Comparison with previous 3D open-vocabulary semantic segmentation methods on ScanNe200. Experimental results demonstrate that our work outperforms the state-of-the-art approaches in terms of AP.

Method	Reference	AP <sub>novel</sub>	AP <sub>base</sub>	AP
OpenScene [36] + Mask3D [43]	CVPR'23	7.6	11.1	8.5
OpenMask3D[48]	NeurIPS'23	11.9	14.3	12.6
SOLE[24]	CVPR'24	<b>19.1</b>	17.4	18.7
Open3DIS[35]	CVPR'24	16.5	<b>25.8</b>	19.0
UniSeg3D (ours)	-	<u>18.0</u>	<u>24.4</u>	<b>19.7</b>

Table III: Comparison with previous 3D interactive segmentation methods on ScanNet. UniSeg3D demonstrates remarkable performance in AP, AP<sub>50</sub> and AP<sub>25</sub>.

Method	Reference	AP	AP <sub>50</sub>	AP <sub>25</sub>
InterObject3D [20]	ICRA'23	20.9	38.0	67.2
AGILE3D [61]	ICLR'24	<u>53.5</u>	<u>75.6</u>	<u>91.3</u>
UniSeg3D (ours)	-	<b>54.5</b>	<b>79.4</b>	<b>93.2</b>

Table IV: Comparison with previous 3D referring segmentation methods on ScanRefer. UniSeg3D demonstrates significant performance in terms of mIoU and acc@0.25

Method	Reference	mIoU	acc@0.5	acc@0.25
TGNN [13]	AAAI'21	24.9	<u>28.2</u>	33.2
X-RefSeg3D [40]	AAAI'24	<u>25.5</u>	<b>28.6</b>	<u>34.0</u>
UniSeg3D (ours)	-	<b>29.6</b>	28.0	<b>41.5</b>



## B Analysis on Inference Time.

This work proposes a unified framework, achieving six tasks in once inference. It is more efficient compared with running six approaches specialized for a single task. We present the inference time of the proposed method for further analysis of efficiency. Tab. V illustrates that our method achieves effective integration across six tasks while maintaining highly competitive inference times compared to previous methods.

Table V: The inference time and instance segmentation accuracy on the ScanNet validation split.

Method	Component	Device	Component time, ms	Total time, ms	mAP
PointGroup [16]	Backbone	GPU	48	372	34.8
	Grouping	GPU+CPU	218		
	ScoreNet	GPU	106		
HAIS [2]	Backbone	GPU	50	256	43.5
	Hierarchical aggregation	GPU+CPU	116		
	Intra-instance refinement	GPU	90		
SoftGroup [49]	Backbone	GPU	48	266	45.8
	Soft grouping	GPU+CPU	121		
	Top-down refinement	GPU	97		
SSTNet [28]	Superpoint extraction	CPU	168	400	49.4
	Backbone	GPU	26		
	Tree Network	GPU+CPU	148		
	ScoreNet	GPU	58		
Mask3D [43] w/o clustering	Backbone	GPU	106	221	54.3
	Mask module	GPU	100		
	Query refinement	GPU	15		
Mask3D [43]	Backbone	GPU	106	19851	55.2
	Mask module	GPU	100		
	Query refinement	GPU	15		
	DBSCAN clustering	CPU	19630		
SPFormer [46]	Superpoint extraction	CPU	168	215	56.3
	Backbone	GPU	26		
	Superpoint pooling	GPU	4		
	Query decoder	GPU	17		
OneFormer3D [19]	Superpoint extraction	CPU	168	221	59.3
	Backbone	GPU	26		
	Superpoint pooling	GPU	4		
	Query decoder	GPU	23		
UniSeg3D(ours)	Superpoint extraction	CPU	168	230.03	59.3
	Backbone	GPU	33		
	Text encoder	GPU	0.03		
	Mask decoder	GPU	29		

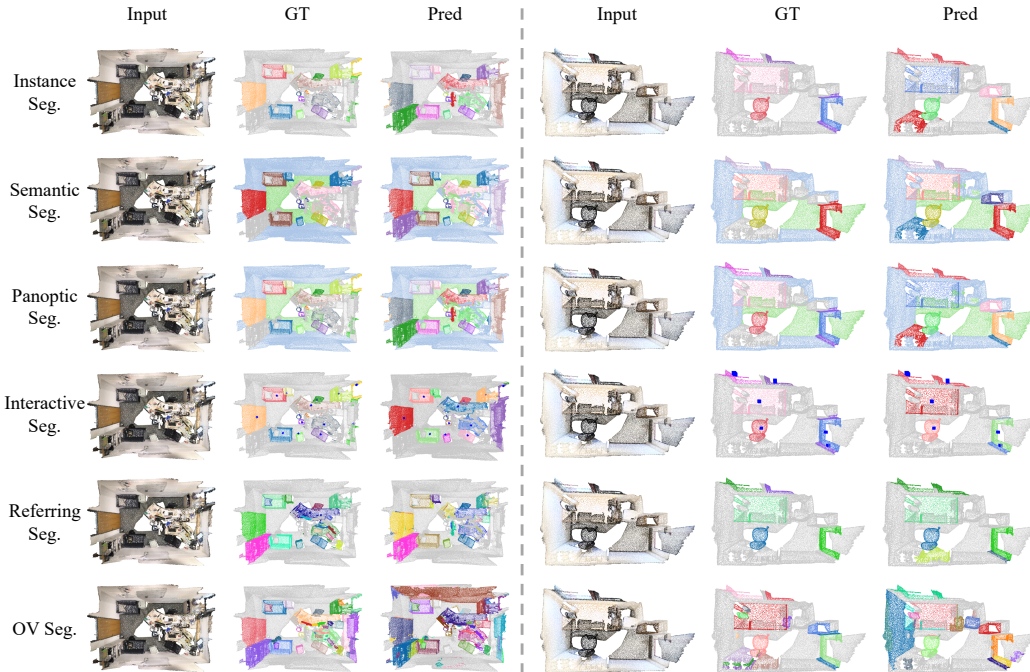


Figure I: Visualization of segmentation results obtained by UniSeg3D on the ScanNet validation split.

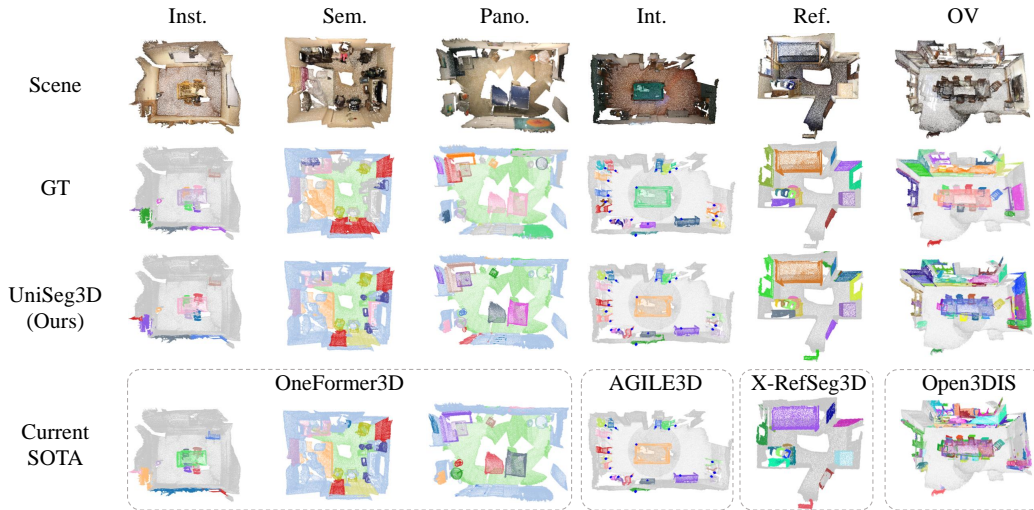


Figure II: Visualization of segmentation results obtained by UniSeg3D and current SOTA methods on the ScanNet validation split.

### C Qualitative Visualizations.

We provide additional qualitative results in this section. In Fig. I, visualizations of segmentation results for additional scenes are presented, showcasing the point clouds, the ground truth, and the segmentation result obtained by UniSeg3D for all 6 tasks within each scene. In Fig. II, we present the visualizations of segmentation results obtained by UniSeg3D and the current SOTA methods on the ScanNet dataset. We list four current methods, including OneFormer3D, AGILE3D, X-RefSeg3D, and Open3DIS, each of which achieved SOTA exclusively within their respective tasks, while UniSeg3D accomplished high-quality segmentation across all tasks.